ELSEVIER

Journal of Fluids and Structures 23 (2007) 391–411

JOURNAL OF FLUIDS AND STRUCTURES

www.elsevier.com/locate/jfs

Numerical simulation of flow induced airfoil vibrations with large amplitudes

P. Sváček[a], M. Feistauer[b], J. Horáček[c,*]

[a]*Faculty of Mechanical Engineering, Czech Technical University Prague, Karlovo nám. 13, 121 35 Praha 2, Czech Republic*
[b]*Faculty of Mathematics and Physics, Charles University Prague, Sokolovská 83, 186 75 Praha 8, Czech Republic*
[c]*Institute of Thermomechanics, Academy of Sciences of the Czech Republic, Dolejškova 5, 182 00 Praha 8, Czech Republic*

Received 28 October 2004; accepted 9 October 2006
Available online 18 December 2006

Abstract

The subject of this paper is the numerical simulation of the interaction of two-dimensional incompressible viscous flow and a vibrating airfoil. A solid airfoil with two degrees of freedom, which can rotate around the elastic axis and oscillate in the vertical direction, is considered. The numerical simulation consists of the finite element solution of the Navier–Stokes equations, coupled with the system of ordinary differential equations describing the airfoil motion. The high Reynolds numbers considered 10^5-10^6 require the application of a suitable stabilization of the finite element discretization. The method presented in this paper is based on the laminar model and the turbulence modelling is not applied here. The time-dependent computational domain and a moving grid are taken into account with the aid of the arbitrary Lagrangian–Eulerian (ALE) formulation of the Navier–Stokes equations. Special attention is paid to the time discretization and the solution of the nonlinear discrete problem on each time level is performed. As a result, a sufficiently accurate and robust method is developed, which is applied to the case of flow-induced airfoil vibrations with large amplitudes after the loss of aeroelastic stability. The computational results are compared with known aerodynamical data and with results of aeroelastic calculations obtained by NASTRAN code for a linear approximation.

Keywords: Aeroelasticity; Flutter; Nonlinear oscillations; Finite element method

1. Introduction

The interaction of fluid flow and an elastic structure plays an important role in many technical disciplines—airplane industry (e.g., wings deformations), bladed machines (turbines, compressors, pumps), civil engineering (stability of bridges), etc. The research in aeroelasticity or hydroelasticity focuses on the interaction between moving fluids and vibrating structures [see, e.g., Dowell (1995), Naudasher and Rockwell (1994)]. Widely used commercial codes, as e.g. NASTRAN, FLUENT or ANSYS, can solve only special problems of aeroelasticity or hydroelasticity and are mainly limited to linearized models. Using NASTRAN, the critical fluid flow velocity can be determined, but the post-flutter

*Corresponding author. Tel.: +420 2 66053125; fax: +420 286 584 695.
E-mail addresses: svacek@marian.fsik.cvut.cz (P. Sváček), feist@karlin.mff.cuni.cz (M. Feistauer), jaromirh@it.cas.cz (J. Horáček).

0889-9746/$ - see front matter © 2006 Elsevier Ltd. All rights reserved.
doi:10.1016/j.jfluidstructs.2006.10.005

Nomenclature

c	airfoil chord (m)	k_{hh}	bending stiffness (N/m)
$D(t)$	aerodynamic drag force (N)	$k_{\alpha\alpha}$	torsional stiffness (N m/rad)
d_{hh}	structural damping in bending (kg/s)	$L(t)$	aerodynamic lift force (upwards positive) (N)
$d_{\alpha\alpha}$	structural damping in torsion ($\mathrm{kg\,m^2/(s\,rad)}$)	l	airfoil depth (m)
EO	elastic axis	$M(t)$	aerodynamic torsional moment (clockwise positive) (N m)
h	vertical displacement of the elastic axis EO (downwards positive) (m)	m	mass of the airfoil (kg)
I_α	inertia moment around the elastic axis EO ($\mathrm{kg\,m^2}$)	S_α	static moment around the elastic axis EO (kg m)
		α	rotational displacement around the elastic axis EO (clockwise positive) (rad)

behaviour and other nonlinear phenomena for large amplitudes of vibration cannot be captured. Since the appearance of any aerodynamic instability is not admissible in normal flight regimes, the nonlinear postcritical limit states usually had not been considered. Recently, the modelling of post-flutter behaviour began to be more important.

Flutter at large deformations can be studied by analytical methods (Holmes and Marsden, 1977) only in some special cases. Nevertheless, the real situation is usually much more complicated. It is necessary to consider viscous flow, changes of the flow domain in time, turbulence effects, nonlinear behaviour of the elastic structure and to solve simultaneously the evolution systems for the fluid flow and for the oscillating structure. Considering the Navier–Stokes equations and a vibrating structure with large displacements, when the change of the fluid domain cannot be neglected, methods with moving meshes must be employed [see, e.g., Farhat et al. (1995), Le Tallec and Mouro (2001)]. Moreover, the application of efficient and robust methods for the numerical solution of the nonlinear Navier–Stokes system is required. The underlying mathematical model depends on the qualitative properties of the fluid flow, and for lower flow velocities the fluid can be treated as incompressible.

Very strong nonlinear self-sustained pitch vibrations of a guide blade of a water turbine were observed, for example, by Půlpitel (1984), when a flexibly supported blade with one degree of freedom (rotation considered only) vibrated near a rigid wall of the water tunnel, where large-scale experiments were realized.

Unsteady flow fields around airfoils oscillating with large amplitudes in pitch motion and associated dynamic stall phenomena were investigated by Tuncer et al. (1990). A viscous flow analysis based on an integro-differential formulation of the Navier–Stokes equations, was developed. The full viscous flow analysis of the NACA 0012 airfoil has shown that the dynamics of the leading-edge vortex has a dominant effect on the dynamic stall behaviour of the system.

The incompressible, viscous flow over two-dimensional elliptic airfoils oscillating in pitch at large angles of attack has been simulated numerically for Reynolds number 3000 by Akbari and Price (2000) with the aid of a vortex-in-cell method.

The existence of limit-cycle oscillations of aeroelastic wing sections with structural nonlinearity was studied by Singh and Brenner (2003). The chosen dynamic model describes the nonlinear plunge and pitch motion of the wing. The limit-cycle calculations and orbital stability analysis were performed. Numerical results show that the predicted limit-cycle oscillation amplitude and frequency correspond approximately to actual values. However, only linear quasi-steady aerodynamic theory was considered in this study.

The possible existence of internal resonance and related nonlinear phenomena was recently published by Gilliatt et al. (2003). The authors showed that, for specific classes of aeroelastic systems with nonlinearities, aeroelastic instabilities may appear which are not predicted by traditional (linear) approaches. The studied system exhibited a resonance behaviour under subcritical conditions.

A new stochastic controller for a dynamic system under irregular sudden disturbance has been developed by Heo et al. (2003). A flutter control simulation for a thin airfoil in turbulent flow was conducted numerically and used for an active suppression of flutter.

The unsteady, incompressible, viscous laminar flow over a pitching NACA 0012 airfoil was numerically simulated for a prescribed frequency of oscillation by Akbari and Price (2003). A vortex method was used to solve the 2-D Navier–Stokes equations in the vorticity/stream-function form. It was observed that the reduced frequency has the main influence on the flow field during dynamic stall of this airfoil.

This paper is focused on the numerical simulation of aeroelastic problem of two-dimensional viscous incompressible air flow and an airfoil with two degrees of freedom. The airfoil is considered as a solid flexibly supported body, allowing vertical and torsional vibrations. Transient motion of the airfoil before or after loss of stability is also addressed.

The mathematical model of the fluid flow is represented by the system consisting of the 2-D Navier–Stokes equations and the continuity equation, equipped with initial conditions and mixed boundary conditions. The incompressible flow problems include a wide range of complications, typical of the numerical solution of singularly perturbed partial differential equations. There exist a number of various numerical techniques for the solution of the Navier–Stokes system. Beside the finite difference method, an alternative is the finite volume method [see, e.g., Fürst et al. (2001), Fořt et al. (2002), Honzátko et al. (2004)], which is rather popular in Computational Fluid Dynamics. However, the construction of higher-order accurate finite volume methods for the solution of incompressible viscous flow is quite difficult.

In the case of flows in domains with complicated geometry and under mixed boundary conditions it appears that it is more suitable to use the finite element method (FEM). It is well-known that FEM can be applied with success to a large variety of problems. However, in the finite element solution of incompressible Navier–Stokes equations one has to overcome several important obstacles. First, it is necessary to take into account that the finite element velocity/pressure pair has to be suitably chosen in order to satisfy the Babuška-Breezi condition, which guarantees the stability of the scheme—see, e.g., Girault and Raviart (1986) or Gresho and Sani (2000). Further, the dominating convection requires the introduction of some stabilization of the finite element scheme, such as upwinding or the streamline-diffusion method (also called SUPG method)—see, e.g., Feistauer et al. (2003, Chapter 4). However, the published stabilized methods can usually be applied with success to problems with Reynolds numbers less than 5×10^4, whereas for the problem studied here the relevant Reynolds numbers are usually in the range $10^5 - 10^6$. In such a case, it is necessary to use a sophisticated choice of stabilization parameters based on a careful theoretical mathematical analysis, as carried out, by Lube (1994) and Gelhard et al. (2005) for example. For a practical implementation in the framework of an aeroelastic problem, see Sváček and Feistauer (2004). Moreover, it is necessary to design carefully the computational mesh, using adaptive grid refinement in order to allow an accurate resolution of time oscillating thin boundary layers, wakes and vortices. In our case we use the anisotropic mesh adaptation technique of Dolejší (2001) for the construction and adaptive refinement of the mesh.

Due to the motion of the airfoil, the computational domain is time-dependent. This requires to use techniques working on moving meshes. A suitable choice is to apply the arbitrary Lagrangian–Eulerian (ALE) method, which is based on the reformulation of the Navier–Stokes equations (Nomura and Hughes, 1992; Le Tallec and Mouro, 2001) using an ALE mapping of the reference configuration onto the current configuration for the time under consideration. The ALE formulation of the Navier–Stokes equations is coupled with the structural model, describing the airfoil vibrations.

The use of FEM leads to a large discrete system of nonlinear algebraic equations. In order to solve the problem in the shortest possible time, a suitable linearization and a sufficiently fast solver has to be applied in each time step. The multilevel methods are usually very efficient for the solution of linear systems arising from discretization of partial differential equations [e.g. multigrid, domain decomposition; see Quarteroni and Valli (1999)]. Although these methods are very efficient for symmetric linear problems, their application to the Navier–Stokes equations is not quite straightforward (Turek, 1999; Otto and Lube, 1998). The situation is even more complicated on unstructured anisotropic grids. Here, a direct solver from Davis and Duff (1999) for linear systems is employed, working sufficiently efficiently for systems with up to 10^5 unknowns.

In the present paper, attention is paid step-by-step to the following aspects: second order time discretization and space finite element discretization of the Navier–Stokes equations, SUPG stabilization of the FEM, the choice of stabilization parameters, discretization of the structural model, numerical realization of the nonlinear discrete problem including the coupling of the fluid flow and airfoil motion. The developed sufficiently accurate and robust method is applied to a technically relevant case of flow-induced airfoil vibrations. The computational results are compared with available aerodynamic and aeroelastic data and NASTRAN code calculations.

2. Formulation of the problem

First we introduce the initial-boundary value problem describing the fluid flow motion, consisting of the continuity equation and the Navier–Stokes equations rewritten in the ALE form, and suitable initial and boundary conditions. Furthermore, we introduce the system of ordinary nonlinear differential equations of airfoil vibrations and formulate the coupling between the moving fluid and vibrating structure.

2.1. Description of the fluid flow

We assume that $(0, T)$ is a time interval and we denote by Ω_t a computational domain occupied by the fluid at time t. We denote by $\boldsymbol{u} = \boldsymbol{u}(x, t)$ and $p = p(x, t)$, $x \in \Omega_t$, $t \in (0, T)$ the flow velocity and the kinematic pressure

(i.e., dynamic pressure divided by the density ρ of the fluid) and ν denotes the kinematic viscosity. We have $\boldsymbol{u} = (u_1, u_2)$, where u_1 and u_2 are the components of the velocity in the directions of the Cartesian coordinates x_1 and x_2 of x. By R and R^2 we denote the set of all real numbers and the set of all two-dimensional vectors, respectively.

In order to simulate flow in a moving domain, we employ the arbitrary Eulerian–Lagrangian (ALE) method, based on an ALE mapping

$$A_t: \Omega_{\text{ref}} \to \Omega_t, \quad X \mapsto x(X,t) = A_t(X), \tag{1}$$

of the reference configuration $\Omega_{\text{ref}} = \Omega_0$ onto the current configuration Ω_t, with the ALE velocity $\boldsymbol{w} = \partial A_t/\partial t$. We suppose that the ALE velocity at each point on the surface of the airfoil is equal to the velocity of its motion. By D^A/Dt we denote the ALE derivative—i.e. the derivative with respect to the reference configuration. The ALE mapping is shown in Fig. 1. In the domain Ω_t we consider the Navier–Stokes system written in the following ALE form, cf. Nomura and Hughes (1992):

$$\frac{D^A}{Dt}\boldsymbol{u} + [(\boldsymbol{u} - \boldsymbol{w}) \cdot \nabla]\boldsymbol{u} + \nabla p - \nu \Delta \boldsymbol{u} = 0, \tag{2}$$

$$\nabla \cdot \boldsymbol{u} = 0, \tag{3}$$

to which we add the initial condition

$$\boldsymbol{u}(x,0) = \boldsymbol{u}_0, \quad x \in \Omega_0, \tag{4}$$

and boundary conditions

$$\begin{aligned} &\text{(a)}\ \ \boldsymbol{u}|_{\Gamma_D} = \boldsymbol{u}_D, \quad \text{(b)}\ \ \boldsymbol{u}|_{\Gamma_{Wt}} = \boldsymbol{w}|_{\Gamma_{Wt}}, \\ &\text{(c)}\ \ -(p - p_{\text{ref}})\boldsymbol{n} + \nu \frac{\partial \boldsymbol{u}}{\partial \boldsymbol{n}} = 0 \quad \text{on } \Gamma_O. \end{aligned} \tag{5}$$

Here $\boldsymbol{n}$ is the unit outer normal to the boundary $\partial\Omega_t$ of the domain Ω_t, Γ_D represents the inlet (and, possibly, fixed impermeable walls), Γ_O is the outlet and Γ_{Wt} is the boundary of the airfoil at time t. Condition (5b) represents the assumption that the fluid adheres to the airfoil. We denote by p_{ref} a prescribed reference outlet pressure. The choice of a suitable boundary condition on the outlet is a delicate question. In order to allow a good resolution of a wake propagation through the outlet, we use here the "soft" boundary condition (5c) [often called the do-nothing condition—see Turek (1999)].

2.2. Description of the airfoil motion

We assume that the airfoil has two degrees of freedom. This means that we consider the airfoil as a solid body, which can oscillate in the vertical direction and in the angular direction around the so-called elastic axis.

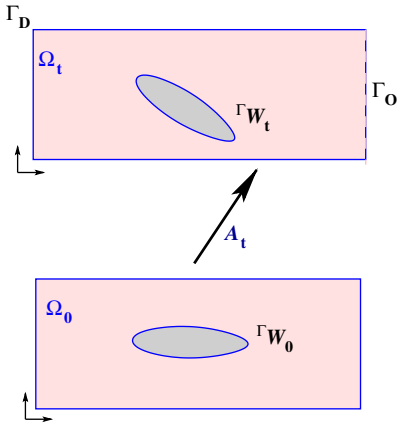

Fig. 1. ALE mapping of the reference configuration Ω_0 onto the current configuration Ω_t.

In order to simulate the airfoil oscillations with large displacements, we include geometrical nonlinearities into the equations of motion, which have the form [see, e.g., Horáček et al. (2003)]

$$m\ddot{h} + k_{hh}h + S_\alpha\ddot{\alpha}\cos\alpha - S_\alpha\dot{\alpha}^2\sin\alpha + d_{hh}\dot{h} = -L(t), \quad S_\alpha\ddot{h}\cos\alpha + I_\alpha\ddot{\alpha} + k_{\alpha\alpha}\alpha + d_{\alpha\alpha}\dot{\alpha} = M(t), \tag{6}$$

where we use the notation defined in the Nomenclature.

The vertical and torsional motion with small vibration amplitudes of the angle α and its derivative $\dot{\alpha}$ is described by the linearized system of ordinary differential equations

$$\begin{aligned} &m\ddot{h} + k_{hh}h + S_\alpha\ddot{\alpha} + d_{hh}\dot{h} = -L(t),\\ &S_\alpha\ddot{h} + I_\alpha\ddot{\alpha} + k_{\alpha\alpha}\alpha + d_{\alpha\alpha}\dot{\alpha} = M(t). \end{aligned} \tag{7}$$

Systems (6) or (7) are equipped with the initial conditions prescribing the values $h(0)$, $\alpha(0)$, $\dot{h}(0)$, $\dot{\alpha}(0)$. Then they are transformed to first-order ODE systems and solved numerically by the fourth-order Runge–Kutta method. The derivation of Eqs. (6) and (7) is given in Appendix A.

The aerodynamic lift force L acting in the vertical direction, the torsional moment M and the drag force D are defined by

$$L = -l\int_{\Gamma_{W_t}}\sum_{j=1}^{2}\tau_{2j}n_j\,\mathrm{d}S, \quad M = +l\int_{\Gamma_{W_t}}\sum_{i,j=1}^{2}\tau_{ij}n_j r_i^{\mathrm{ort}}\,\mathrm{d}S, \quad D = -l\int_{\Gamma_{W_t}}\sum_{j=1}^{2}\tau_{1j}n_j\,\mathrm{d}S, \tag{8}$$

where

$$\tau_{ij} = \rho\left[-p\delta_{ij} + \nu\left(\frac{\partial u_i}{\partial x_j} + \frac{\partial u_j}{\partial x_i}\right)\right], \quad r_1^{\mathrm{ort}} = -(x_2 - x_{\mathrm{EO2}}), \quad r_2^{\mathrm{ort}} = x_1 - x_{\mathrm{EO1}}, \tag{9}$$

By τ_{ij} we denote the components of the stress tensor, δ_{ij} denotes the Kronecker symbol, $\boldsymbol{n} = (n_1, n_2)$ is the unit outer normal to $\partial\Omega_t$ on Γ_{W_t} (pointing into the airfoil) and $x_{\mathrm{EO}} = (x_{\mathrm{EO1}}, x_{\mathrm{EO2}})$ is the position of the elastic axis (lying in the interior of the airfoil). Relations (8) and (9) define the coupling of the fluid dynamical model with the structural model. In Section 3.4 we shall present an efficient method of the calculation of the quantities L and M.

3. Discretization of the Navier–Stokes equations

3.1. Time discretization

First let us describe the time discretization of the problem. We consider a partition $0 = t_0 < t_1 < \cdots < T$, $t_k = k\tau$, with a time step $\tau > 0$, of the time interval $[0, T]$ and approximate the solution $\boldsymbol{u}(t_n)$ (defined in Ω_{t_n}) at time t_n by $\boldsymbol{u}^n$. For the time discretization we use a second-order two-step scheme using the computed approximate solution $\boldsymbol{u}^{n-1}$ in $\Omega_{t_{n-1}}$ and $\boldsymbol{u}^n$ in Ω_{t_n} for the calculation of $\boldsymbol{u}^{n+1}$ in the domain $\Omega_{t_{n+1}}$. We approximate the ALE velocity $\boldsymbol{w}(t_{n+1})$ by $\boldsymbol{w}^{n+1}$ and set $\hat{\boldsymbol{u}}^i = \boldsymbol{u}^i \circ A_{t_i} \circ A_{t_{n+1}}^{-1}$ (the symbol $\circ$ denotes the composite function). The vector-valued functions $\hat{\boldsymbol{u}}^i$ are defined in the domain $\Omega_{t_{n+1}}$.

Then, on each time level t_{n+1}, the second-order two-step ALE time discretization yields the problem of finding unknown functions $\boldsymbol{u}^{n+1} : \Omega_{t_{n+1}} \to R^2$ and $p^{n+1} : \Omega_{t_{n+1}} \to R$ satisfying the equations

$$\frac{3\boldsymbol{u}^{n+1} - 4\hat{\boldsymbol{u}}^n + \hat{\boldsymbol{u}}^{n-1}}{2\tau} + ((\boldsymbol{u}^{n+1} - \boldsymbol{w}^{n+1})\cdot\nabla)\boldsymbol{u}^{n+1} - \nu\Delta\boldsymbol{u}^{n+1} + \nabla p^{n+1} = 0, \quad \mathrm{div}\,\boldsymbol{u}^{n+1} = 0, \tag{10}$$

in $\Omega_{t_{n+1}}$, and the boundary conditions (5).

3.2. Space discretization

The starting point for the finite element discretization of problem (10) with the boundary conditions (5) is the so-called weak formulation. To this end we introduce the simplified notation $\Omega := \Omega_{t_{n+1}}$, $\boldsymbol{u} := \boldsymbol{u}^{n+1}$, $p := p^{n+1}$ and write system (10) in the form

$$\frac{3\boldsymbol{u} - 4\hat{\boldsymbol{u}}^n + \hat{\boldsymbol{u}}^{n-1}}{2\tau} + ((\boldsymbol{u} - \boldsymbol{w}^{n+1})\cdot\nabla)\boldsymbol{u} - \nu\Delta\boldsymbol{u} + \nabla p = 0, \quad \mathrm{div}\,\boldsymbol{u} = 0, \tag{11}$$

considered with the boundary conditions (5). Moreover, we define the velocity spaces W, X and the pressure space Q:

$$W = (H^1(\Omega))^2, \quad X = \{\boldsymbol{v} \in W; \boldsymbol{v}|_{\Gamma_D \cup \Gamma_{W_I}} = 0\}, \tag{12}$$

$$Q = L^2(\Omega), \tag{13}$$

where $L^2(\Omega)$ is the Lebesgue space of square integrable functions over the domain Ω, and $H^1(\Omega)$ is the Sobolev space of square integrable functions together with their first order derivatives.

Now, if we multiply the first and second equation in (11) by any function $\boldsymbol{v} \in X$ and $q \in Q$, respectively, sum them, integrate over Ω, transform the terms containing $\Delta \boldsymbol{u}$ and ∇p with the aid of Green's theorem and use the boundary condition (5c), we find that the solution $U = (\boldsymbol{u}, p)$ of the problem of Eqs. (11) and (5) satisfies the condition

$$a(U, U, V) = f(V) \quad \text{for all } V = (\boldsymbol{v}, q) \in X \times Q, \tag{14}$$

and conditions (5a,b). (The boundary condition (5c) is hidden in the identity (14).) Denoting by

$$(\alpha, \beta)_\omega = \int_\omega \alpha\beta \, \mathrm{d}x, \tag{15}$$

the scalar product in $L^2(\omega)$ for some set ω, we can write

$$\begin{aligned} a(U^*, U, V) &= \frac{3}{2\tau}(\boldsymbol{u}, \boldsymbol{v})_\Omega + \nu(\nabla \boldsymbol{u}, \nabla \boldsymbol{v})_\Omega + (((\boldsymbol{u}^* - \boldsymbol{w}^{n+1}) \cdot \nabla)\boldsymbol{u}, \boldsymbol{v})_\Omega - (p, \nabla \cdot \boldsymbol{v})_\Omega + (\nabla \cdot \boldsymbol{u}, q)_\Omega, \\ f(V) &= \frac{1}{2\tau}(4\hat{\boldsymbol{u}}^n - \hat{\boldsymbol{u}}^{n-1}, \boldsymbol{v})_\Omega - \int_{\Gamma_O} p_{\mathrm{ref}} \boldsymbol{v} \cdot \boldsymbol{n} \, \mathrm{d}S, \quad U = (\boldsymbol{u}, p), \quad V = (\boldsymbol{v}, q), \quad U^* = (\boldsymbol{u}^*, p). \end{aligned} \tag{16}$$

In order to apply the Galerkin FEM, we approximate the spaces W, X, Q from the weak formulation by finite dimensional subspaces W_Δ, X_Δ, Q_Δ, $\Delta \in (0, \Delta_0)$, $\Delta_0 > 0$, $X_\Delta = \{\boldsymbol{v}_\Delta \in W_\Delta; \boldsymbol{v}_\Delta|_{\Gamma_D \cup \Gamma_{W_I}} = 0\}$. Hence, we define the *discrete problem* to find an approximate solution $U_\Delta = (\boldsymbol{u}_\Delta, p_\Delta) \in W_\Delta \times Q_\Delta$ such that $\boldsymbol{u}_\Delta$ satisfies approximately conditions (5a,b) and the identity

$$a(U_\Delta, U_\Delta, V_\Delta) = f(V_\Delta) \quad \text{for all } V_\Delta = (\boldsymbol{v}_\Delta, q_\Delta) \in X_\Delta \times Q_\Delta. \tag{17}$$

The couple (X_Δ, Q_Δ) of the finite element spaces should satisfy the Babuška–Brezzi (BB) condition [see, e.g., Girault and Raviart (1986), Gresho and Sani (2000), and Verfürth (1984)]. In practical computations we assume that the domain Ω is a polygonal approximation of the region occupied by the fluid at time t_{n+1} and the spaces W_Δ, X_Δ, Q_Δ are defined over a triangulation T_Δ of the domain Ω, formed by a finite number of closed triangles $K \in T_\Delta$. Here Δ denotes the size of the mesh T_Δ. The spaces W_Δ, X_Δ and Q_Δ are formed by piecewise polynomial functions. In our computations, the well-known Taylor–Hood P_2/P_1 conforming elements are used for the velocity/pressure approximation. This means that p_Δ is a linear function and $\boldsymbol{u}_\Delta$ is a quadratic vector-valued function on each element $K \in T_\Delta$.

3.3. Stabilization of the FEM

The standard Galerkin discretization (17) may produce approximate solutions suffering from spurious oscillations for high Reynolds numbers. In order to avoid this drawback, the *stabilization via streamline-diffusion/Petrov–Galerkin technique* is applied [see, e.g., Lube (1994), Gelhard et al. (2005)]. The stabilization terms are defined as

$$\begin{aligned} L_\Delta(U^*, U, V) &= \sum_{K \in T_\Delta} \delta_K \left(\frac{3}{2\tau}\boldsymbol{u} - \nu\Delta\boldsymbol{u} + (\tilde{\boldsymbol{w}} \cdot \nabla)\boldsymbol{u} + \nabla p, (\tilde{\boldsymbol{w}} \cdot \nabla)\boldsymbol{v} \right)_K, \\ F_\Delta(V) &= \sum_{K \in T_\Delta} \delta_K \left(\frac{1}{2\tau}(4\hat{\boldsymbol{u}}^n - \hat{\boldsymbol{u}}^{n-1}), (\tilde{\boldsymbol{w}} \cdot \nabla)\boldsymbol{v} \right)_K, \quad U = (\boldsymbol{u}, p), \quad V = (\boldsymbol{v}, q), \quad U^* = (\boldsymbol{u}^*, p), \end{aligned} \tag{18}$$

where the function $\tilde{\boldsymbol{w}}$ stands for the transport velocity, i.e. $\tilde{\boldsymbol{w}} = \boldsymbol{u}^* - \boldsymbol{w}^{n+1}$, $(\cdot, \cdot)_K$ denotes the scalar product in $L^2(K)$, defined by (15), and $\delta_K \geqslant 0$ are suitably chosen parameters. Moreover, the additional grad-div stabilization

$$P_\Delta(U, V) = \sum_{K \in T_\Delta} \tau_K (\nabla \cdot \boldsymbol{u}, \nabla \cdot \boldsymbol{v})_K, \quad U = (\boldsymbol{u}, p), \quad V = (\boldsymbol{v}, q), \tag{19}$$

is introduced with suitably chosen parameters $\tau_K \geqslant 0$.

The *stabilized discrete problem* reads: Find $U_\Delta = (\boldsymbol{u}_\Delta, p_\Delta) \in W_\Delta \times Q_\Delta$ such that $\boldsymbol{u}_\Delta$ satisfies approximately conditions (5)(a), (b) and

$$a(U_\Delta, U_\Delta, V_\Delta) + L_\Delta(U_\Delta, U_\Delta, V_\Delta) + P_\Delta(U_\Delta, V_\Delta) = f(V_\Delta) + F_\Delta(V_\Delta) \quad \text{for all } V_\Delta = (\boldsymbol{v}_\Delta, q_\Delta) \in X_\Delta \times Q_\Delta. \tag{20}$$

The choice of the parameters δ_K and τ_K is carried out according to Lube (1994) or Sváček and Feistauer (2004). The parameter δ_K is defined on the basis of the local transport velocity $\tilde{\boldsymbol{w}}$, namely,

$$\delta_K = \delta^* \frac{h_K}{2\|\tilde{\boldsymbol{w}}\|_{\infty,K}} \xi(\mathrm{Re}_{\tilde{\boldsymbol{w}}}), \tag{21}$$

where

$$\mathrm{Re}_{\tilde{\boldsymbol{w}}} = \frac{h_K \|\tilde{\boldsymbol{w}}\|_{\infty,K}}{2\nu} \tag{22}$$

is the local Reynolds number and h_K is the size of the element K measured in the direction of $\tilde{\boldsymbol{w}}$ and the symbol $\|\cdot\|_{\infty,K}$ denotes the norm in the space $L^\infty(K)$:

$$\|\tilde{\boldsymbol{w}}\|_{\infty,K} = \max_K |\tilde{\boldsymbol{w}}|. \tag{23}$$

The factor $\xi(\cdot)$ is defined by

$$\xi(\mathrm{Re}_{\tilde{\boldsymbol{w}}}) = \min\left(\frac{\mathrm{Re}_{\tilde{\boldsymbol{w}}}}{6}, 1\right). \tag{24}$$

It appears that for P_2/P_1 elements it is possible to set $\tau_K \approx 1$ for all $K \in T_\Delta$.

The nonlinear algebraic discrete system (20) is solved on each time level t_{n+1} with the aid of the linearized Oseen iterative process

$$a(U_\Delta^{(\ell)}, U_\Delta^{(\ell+1)}, V_\Delta) + L_\Delta(U_\Delta^{(\ell)}, U_\Delta^{(\ell+1)}, V_\Delta) + P_\Delta(U_\Delta^{(\ell+1)}, V_\Delta) = f(V_\Delta) + F_\Delta(V_\Delta) \quad \text{for all } V_\Delta \in X_\Delta \times Q_\Delta, \tag{25}$$

where we start from the initial approximation $U_\Delta^{(0)} = (\hat{\boldsymbol{u}}^n, \hat{p}^n)$ or $U_\Delta^{(0)} = (2\hat{\boldsymbol{u}}^n - \hat{\boldsymbol{u}}^{n-1}, 2\hat{p}^n - \hat{p}^{n-1})$. It is enough to compute 5–8 Oseen iterations on each time level.

The solution of the linearized algebraic systems equivalent to (25) is realized by the direct solver UMFPACK (Davis and Duff, 1999), which works sufficiently fast for systems with up to 10^5 equations. For larger systems it is necessary to apply more robust and efficient iterative techniques, such as the domain decomposition approach and/or the multigrid method.

The computational process proceeds in such a way that the computed approximate solution U_Δ of problem (20) on time levels t_n and t_{n-1} and the corresponding force F and moment M are extrapolated and used for obtaining h and α at time t_{n+1} by the fourth-order Runge–Kutta method. This allows us to determine the mapping $A_{t_{n+1}}$ of the reference domain Ω_{ref} onto the domain $\Omega_{t_{n+1}}$ and to approximate the ALE velocity $\boldsymbol{w}^{n+1}$. Then the solution of problem (20) is performed on the next time level t_{n+1}. In order to increase the stability of the process in the case of large far field velocities, a small proportional viscous damping was introduced into systems (6) and (7). Namely, we add the term $\varepsilon k_{hh}\dot{h}$ and $\varepsilon k_{\alpha\alpha}\dot{\alpha}$ to the left-hand side of the first equation and the second equation, respectively, of systems (6) and (7), with $0 < \varepsilon \ll 1$.

3.4. Computation of the force L and moment M

The evaluation of the lift L and the moment M at time $t = t_{n+1}$ from the approximate solution $U_\Delta = (\boldsymbol{u}_\Delta, p_\Delta)$ computed as the solution of the stabilized discrete problem (20) can be carried out in two ways:

(a) One possibility is to compute the components τ_{ij} of the stress tensor at time $t := t_{n+1}$ from formula (9) on the elements $K \in T_\Delta$ adjacent to the airfoil Γ_{Wt}, extrapolate τ_{ij} to the airfoil Γ_{Wt} and then to compute L and M by the integration along Γ_{Wt} according to (8).

(b) More accurate approach, which fits better for the weak formulation of the problem, can be obtained in the following way. The Navier–Stokes equations in the ALE form discretized with respect to time at instant $t := t_{n+1}$ can be expressed component-wise as

$$\frac{3u_i - 4\hat{u}_i^n + \hat{u}_i^{n-1}}{2\tau} + ((\boldsymbol{u} - \boldsymbol{w}^{n+1}) \cdot \nabla)u_i = \sum_{j=1}^{2} \frac{\partial \tau_{ij}}{\partial x_j} \quad \text{in } \Omega_t, \quad i = 1, 2. \tag{26}$$

Let us set

$$\Omega_{\Gamma_{Wt}} = \cup\{K \in T_\Delta; \quad K \cap \Gamma_{Wt} \neq \emptyset\}. \tag{27}$$

This represents a one layer strip around the airfoil formed by finite elements. Multiplying Eq. (26) with $i=2$ by a function $\varphi \in W_{\Delta}$ such that

$$\varphi(x)=1 \quad \text{for } x \in \Gamma_{Wt}, \quad \varphi(x)=0 \quad \text{outside the set } \Omega_{\Gamma_{Wt}}, \tag{28}$$

integrating over $\Omega_{\Gamma_{Wt}}$, applying Green's theorem to the terms with τ_{ij} and, finally, writing the already known finite element approximations $\boldsymbol{u}_{\Delta}$, $\boldsymbol{u}_{\Delta}^{n}$ and $\boldsymbol{u}_{\Delta}^{n-1}$ instead of the functions $\boldsymbol{u}, \boldsymbol{u}^{n}$ and $\boldsymbol{u}^{n-1}$, respectively, we arrive at the representation of the force L:

$$\frac{L}{l}=-\int_{\Omega_{\Gamma_{Wt}}}\left(\frac{3u_{\Delta 2}-4\hat{u}_{\Delta 2}^{n}+\hat{u}_{\Delta 2}^{n-1}}{2\tau}+((\boldsymbol{u}_{\Delta}-\boldsymbol{w}^{n+1})\cdot\nabla)u_{\Delta 2}\right)\varphi-\sum_{j=1}^{2}\tau_{2j}\frac{\partial\varphi}{\partial x_j}\,\mathrm{d}x. \tag{29}$$

(Here we use the notation $\boldsymbol{u}_{\Delta}=(u_{\Delta 1}, u_{\Delta 2})$, $\hat{\boldsymbol{u}}_{\Delta}^{n}=(\hat{u}_{\Delta 1}^{n}, \hat{u}_{\Delta 2}^{n})$, etc.)

Similarly, if we use the vector-valued function $\mathbf{v}^{\mathbf{ort}}=(v_1^{\mathrm{ort}}, v_2^{\mathrm{ort}})=\varphi(r_1^{\mathrm{ort}}, r_2^{\mathrm{ort}})$, where the functions $r_1^{\mathrm{ort}}, r_2^{\mathrm{ort}}$ are defined by (9), we can derive the formula

$$\frac{M}{l}=+\int_{\Omega_{\Gamma_{Wt}}}\left(\frac{3\boldsymbol{u}_{\Delta}-4\hat{\boldsymbol{u}}_{\Delta}^{n}+\hat{\boldsymbol{u}}_{\Delta}^{n-1}}{2\tau}+((\boldsymbol{u}_{\Delta}-\boldsymbol{w}^{n+1})\cdot\nabla)\boldsymbol{u}_{\Delta}\right)\cdot\mathbf{v}^{\mathbf{ort}}\,\mathrm{d}x+\int_{\Omega_{\Gamma_{Wt}}}\sum_{i,j=1}^{2}\tau_{ij}\frac{\partial v_i^{\mathrm{ort}}}{\partial x_j}\,\mathrm{d}x. \tag{30}$$

4. Numerical results

In this section we shall present several computational examples in order to show the applicability of the described method.

4.1. Validation of the method

In order to validate the presented technique, we compare our computations with some experimental results.

First, we define the stationary aerodynamic quantities—the lift coefficient

$$c_L=\frac{L}{\frac{1}{2}\rho U_{\infty}^2 lc}, \tag{31}$$

the drag coefficient

$$c_D=\frac{D}{\frac{1}{2}\rho U_{\infty}^2 lc}, \tag{32}$$

and the torsional moment coefficient

$$c_M=\frac{M}{\frac{1}{2}\rho U_{\infty}^2 lc^2}, \tag{33}$$

and show the comparison of the time averaged coefficients c_L and c_M as a function of the angle of attack, computed for a fixed airfoil NACA 63_2−415 in the case of the Reynolds number $\mathrm{Re}=8\times10^5$, with experimental results from NACA (1945), see Figs. 2 and 3. Fig. 4 shows the dependence of c_D on c_L in comparison with results from NACA (1945). We see a very good agreement for c_L and c_M, which is necessary for the accuracy of the developed coupled fluid-structure interaction computational technique. The differences between the computed and measured values of the drag coefficient c_D are due to several reasons. It is well-known that the precise computation of the drag is rather difficult and requires a very good and fine mesh. Moreover, for the high Reynolds numbers considered it might be necessary to apply a suitable model of turbulence. On the other hand, the drag values are not crucial for our aeroelastic computations.

Further, numerical simulation of flow past the NACA0012 profile with a prescribed vibration around the elastic axis was carried out. The profile rotation was considered according to the formula $\alpha=10(1+\sin(2\pi t/f))$ with frequency $f=U_{\infty}/(2\pi c)$, where c is the airfoil chord and the Reynolds number $\mathrm{Re}=5\times10^3$. The elastic axis was located at 25% of the chord measured from the leading edge. This type of process was examined experimentally and the results are contained in Naudasher and Rockwell (1994, Section 7.3.2). In Figs. 5(a)–(f) we present flow patterns, which we computed for several angles of attack. The agreement with experimental results from Naudasher and Rockwell (1994) is very good.

Finally, we give here the comparison of computed pressure coefficients for the NACA0012 profile with theoretical and experimental results from Triebstein (1986) and Benetka et al. (1998). The chord of the airfoil $c=0.1322\,m$, the

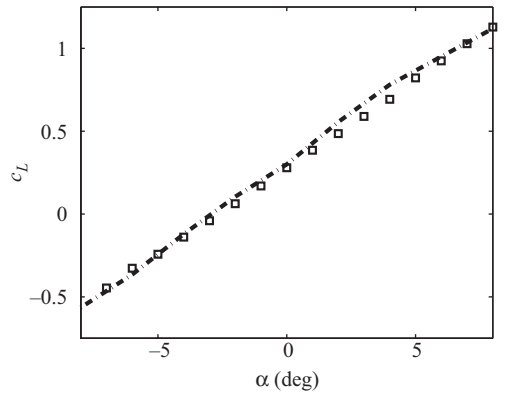

Fig. 2. Comparison of experimental values of the lift coefficient c_L with computed time-averaged values in dependence on the angle of attack α for a fixed nonoscillating airfoil. (Squares denote the computed quantities.)

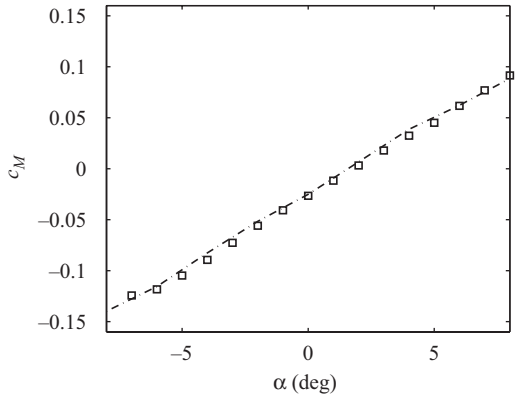

Fig. 3. Comparison of experimental values of the torsional moment coefficient c_M with computed time-averaged values in dependence on the angle of attack α for a fixed nonoscillating airfoil. (Squares denote the computed quantities.)

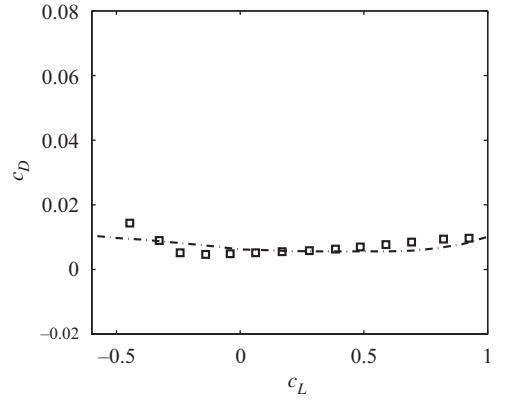

Fig. 4. Comparison of experimental values of the drag coefficient c_D with computed time-averaged values in dependence on the lift coefficient c_L for a fixed nonoscillating airfoil. (Squares denote the computed quantities.)

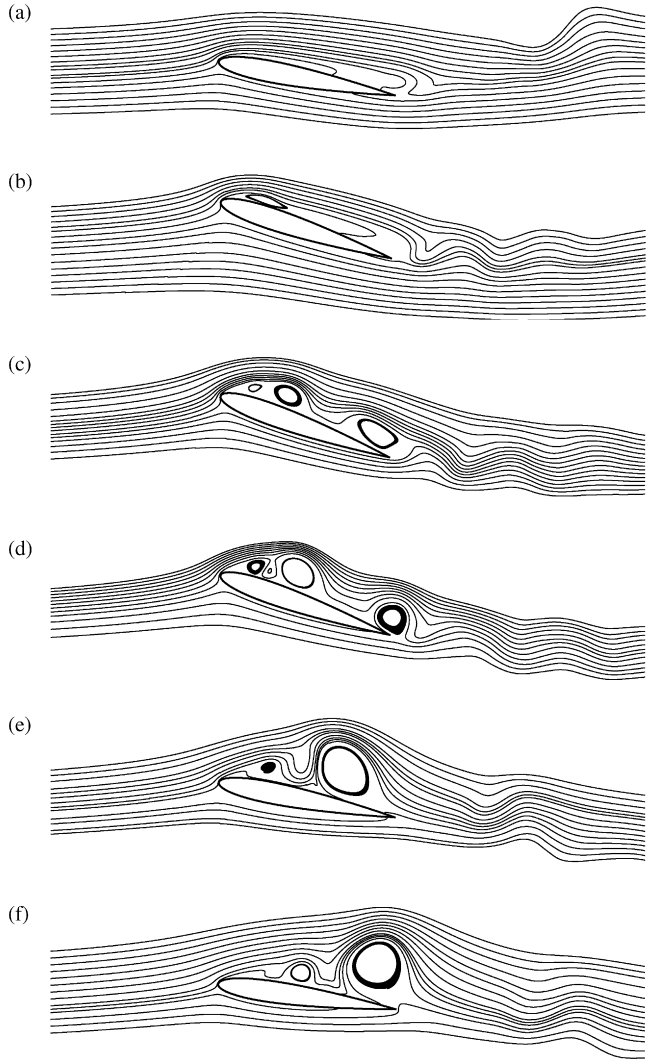

Fig. 5. Streamlines of the flow around a moving airfoil for an angle of attack: (a) $\alpha = 10.86^\circ$; (b) $\alpha = 18.34^\circ$; (c) $\alpha = 20^\circ$; (d) $\alpha = 19.46^\circ$; (e) $\alpha = 12.05^\circ$; and (f) $\alpha = 7.74^\circ$.

prescribed oscillations are defined by $\alpha = \alpha_0 \sin(2\pi t/f)$, the frequency $f = 30\,\mathrm{Hz}$, the far-field velocity $U_\infty = 136\,\mathrm{m/s}$ and the elastic axis is located at 25% of the chord measured from the leading edge.

In Figs. 6 and 7, we present the distribution of the mean value of the pressure coefficient c_p, its real part c_p' and imaginary part c_p'' in dependence on the length of the chord measured from the leading edge for $\alpha_0 = 1^\circ$. The data are scaled to the pitching oscillation amplitude one radian and far field Mach number $\mathrm{Ma} = 0.4$ according to the Prandtl–Glauert formula

$$c_{p\ \mathrm{comp}} = \frac{c_{p\ \mathrm{incomp}}}{\sqrt{1 - \mathrm{Ma}^2}}. \tag{34}$$

4.2. Modelling of flow induced airfoil vibrations

This section presents results of the numerical simulation of flow induced vibrations obtained for the airfoil NACA $63_2 - 415$. The following quantities are considered: $m = 0.086622\,\mathrm{kg}$, $S_\alpha = -0.000779673\,\mathrm{kg\,m}$, $I_\alpha = 0.000487291\,\mathrm{kg\,m^2}$, $k_{hh} = 105.109\,\mathrm{N/m}$, $k_{\alpha\alpha} = 3.695582\,\mathrm{N\,m/rad}$, $l = 0.05\,\mathrm{m}$, $c = 0.3\,\mathrm{m}$, $\rho = 1.225\,\mathrm{kg/m^3}$, $v = 1.5 \times 10^{-5}\,\mathrm{m/s^2}$. The

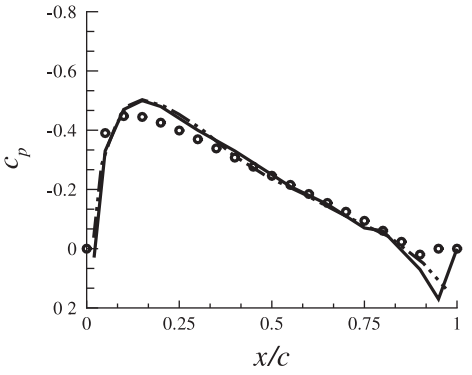

Fig. 6. The mean value of the pressure coefficient c_p for $\alpha_0 = 1^\circ$: ○, computed values; ——, Triebstein experiment; –··–, Benetka experiment.

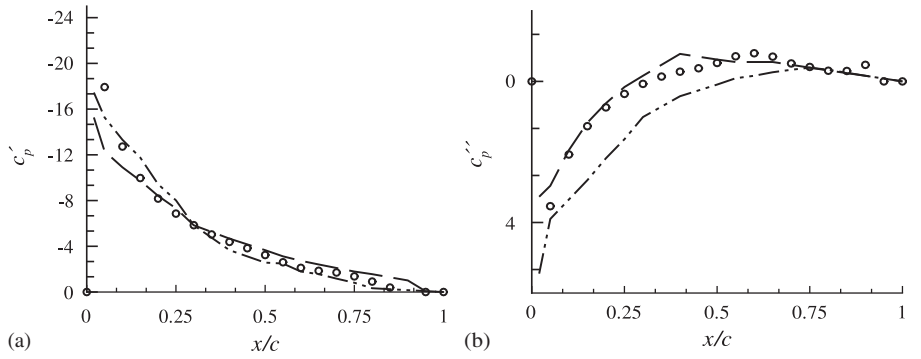

Fig. 7. (a) Real part c_p' and (b) imaginary part c_P'' for $\alpha_0 = 1^\circ$: ○, computed values; ——, Triebstein theory; –··–, Triebstein experiment.

position of the elastic axis EO and the centre of gravity T of the airfoil measured along the chord from the leading edge are $x_{EO} = 0.4c = 0.12\,\text{m}$ and $x_T = 0.37c = 0.111\,\text{m}$, respectively. (See Fig. A1 in Appendix A.) The coefficients of the proportional damping are considered in the form $d_{hh} = \varepsilon k_{hh}$ and $d_{\alpha\alpha} = \varepsilon k_{\alpha\alpha}$, where we choose $\varepsilon = 10^{-3}$.

The far-field flow velocity is considered in the range $U_\infty = 2 - 50\,\text{m/s}$, which yields the Reynolds number $\text{Re} = U_\infty c/\nu$ in the range $4 \times 10^4 - 10^6$. Although the numerical scheme presented above can be applied on any triangular mesh, accurate correct results are conditioned by the use of a mesh sufficiently refined in regions of strong gradients, e.g. in a boundary layer and wake. The anisotropic mesh generator from Dolejší (2001) was employed for the adaptive mesh refinement and the resulting mesh was adapted to the solution behaviour. Fig. 8 shows the computational domain with the used triangulation (at time $t = 0$) consisting of 27 982 triangles (with 14 167 vertices) for the far field velocity $U_\infty = 10\,\text{m/s}$ (i.e. $\text{Re} = 2 \times 10^5$). In Fig. 9 we see details of the mesh in the vicinity of the airfoil.

The computational process for the solution of the nonstationary problem is based on the coupling of the fluid flow problem in the discrete form (20) with the numerical solution of the nonlinear structural model (6). It starts at a certain time $\delta t < 0$ by the solution of the flow, keeping the airfoil in a fixed position given by the prescribed initial translation h_0 and the angle of attack α_0. Then, at time $t = 0$ the airfoil is released and we continue by the solution of a complete fluid–structure interaction problem with $h(0) = h_0 = -50\,\text{mm}$, $\dot{h}(0) = 0$, $\alpha(0) = \alpha_0 = 6^\circ$, $\dot{\alpha}(0) = 0$. In the force L and the moment M appearing in system (6) the static components are compensated. This means that we set $L := L - L_0$, $M := M - M_0$, where the static quantities L_0 and M_0 are obtained from experimental data shown in Figs. 2 and 3, respectively, for the angle of attack $\alpha = 0$.

The simulation of fluid-structure interaction as a function of time is shown in Figs. 10 (a)–(k) for the far-field velocity $U_\infty = 2$, 8, 14, 20, 26, 32, 36, 38, 40, 42 and 45 m/s. The left and right panels show the angle of rotation α and the vertical displacement h, respectively, in dependence on time. In the case of flow velocity 45 m/s, the smaller initial values for the rotational and vertical displacements were chosen, because for larger initial values the vibration amplitudes were increasing very fast.

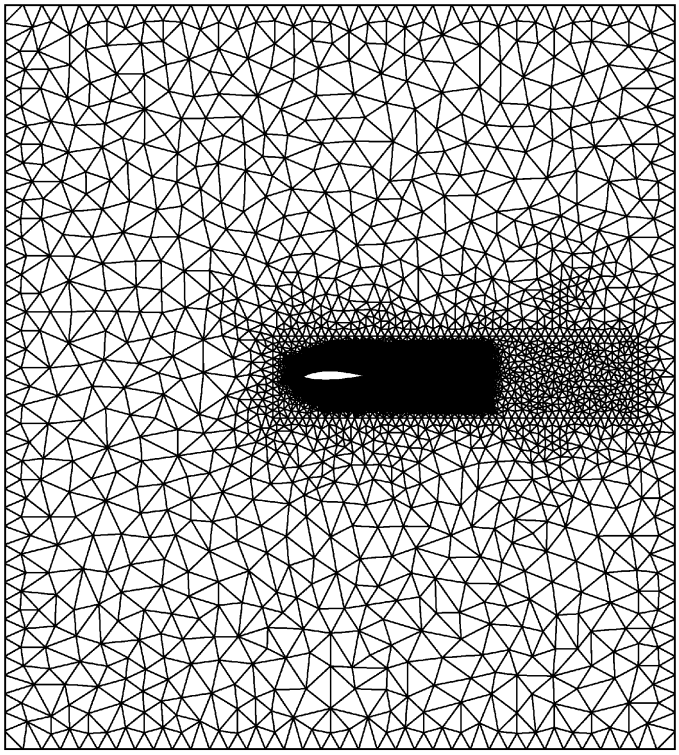

Fig. 8. Triangulation of the computational domain at time $t = 0$.

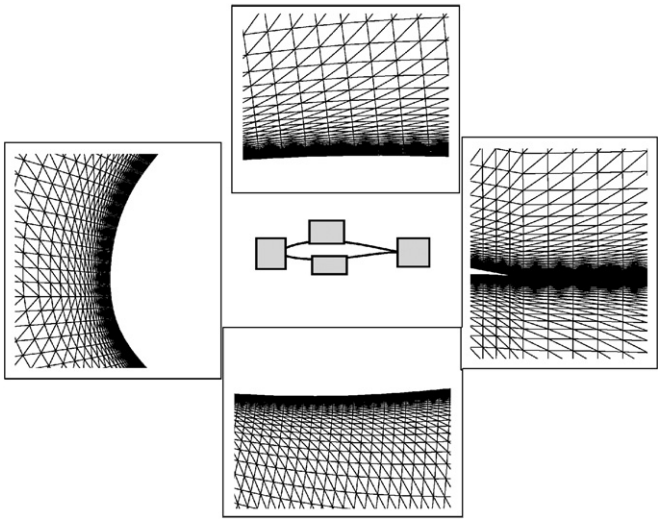

Fig. 9. Details of the mesh.

For the far-field velocity not exceeding 32 m/s the vibrations die out in time and the system is stable. Moreover, we can see that the oscillations are more damped for larger values of the far-field velocity due to the aerodynamic forces. For flow velocities higher than 32 m/s, one can observe the influence of vortices separating from the airfoil. This is seen particularly in the angle α. On the other hand, for $U_\infty \geqslant 40$ m/s we get an unstable behaviour with large airfoil displacements up to 160 mm in the vertical direction, and up to 16° in the rotation. This regime resembles a limit cycle

for postcritical nonlinear oscillations. For $U_\infty = 45\,\mathrm{m/s}$ we get an unstable process with a fast increase of the vibration amplitude.

In Čečrdle and Maleček (2002), the NASTRAN flutter analysis carried out with the aid of the strip model for the fluid flow is presented. The NASTRAN calculations are summarized in Table 1. According to this table the critical velocities are $U_\infty = 37.7\,\mathrm{m/s}$ for divergence and $U_\infty = 42.4\,\mathrm{m/s}$ for flutter, which correspond to our results. Large

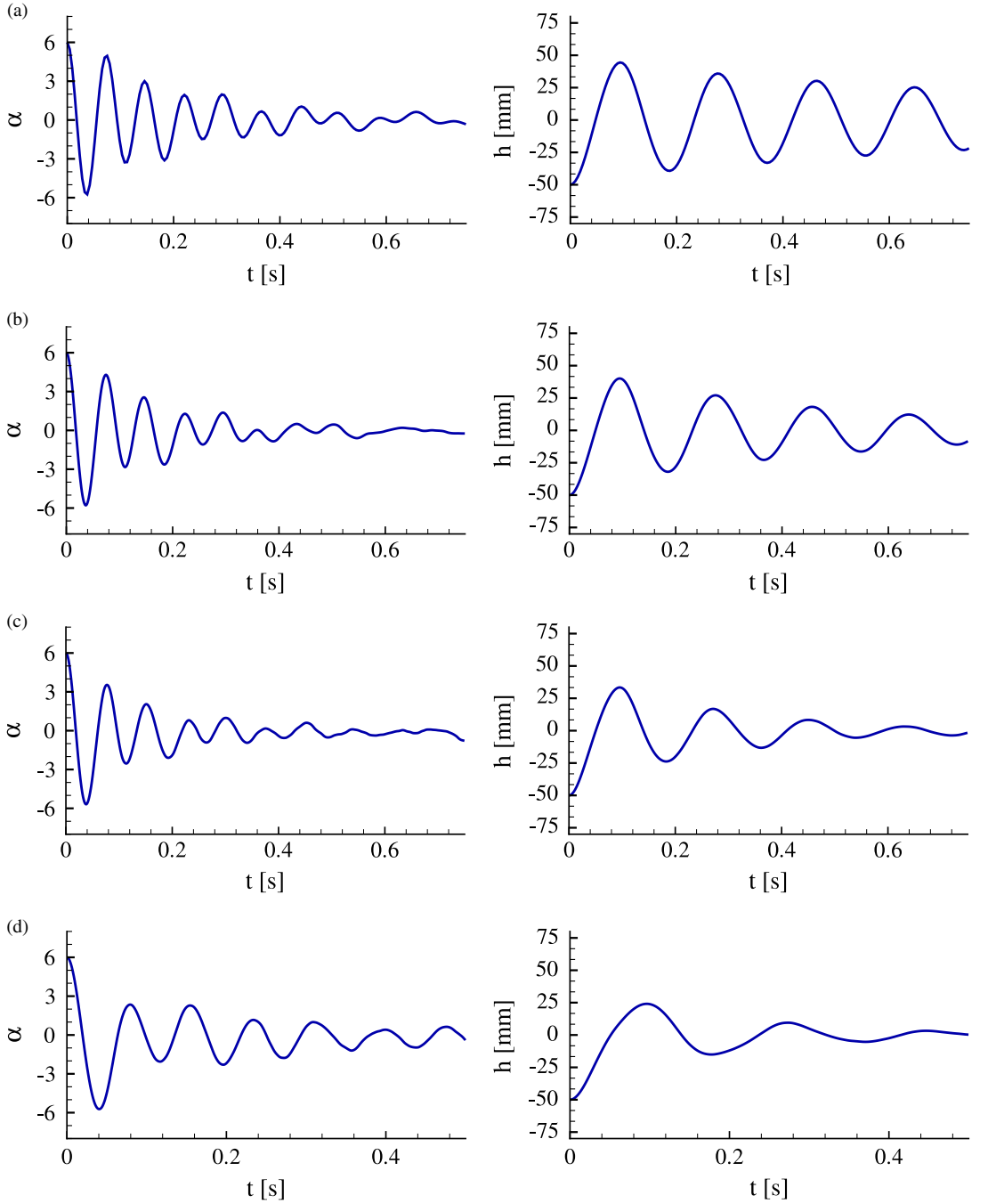

Fig. 10. System response for: (a) $U_\infty = 2\,\mathrm{m/s}$; (b) $U_\infty = 8\,\mathrm{m/s}$; (c) $U_\infty = 14\,\mathrm{m/s}$; (d) $U_\infty = 20\,\mathrm{m/s}$; (e) $U_\infty = 26\,\mathrm{m/s}$; (f) $U_\infty = 32\,\mathrm{m/s}$; (g) $U_\infty = 36\,\mathrm{m/s}$; (h) $U_\infty = 38\,\mathrm{m/s}$; (i) $U_\infty = 40\,\mathrm{m/s}$; (j) $U_\infty = 42\,\mathrm{m/s}$; and (k) $U_\infty = 45\,\mathrm{m/s}$.

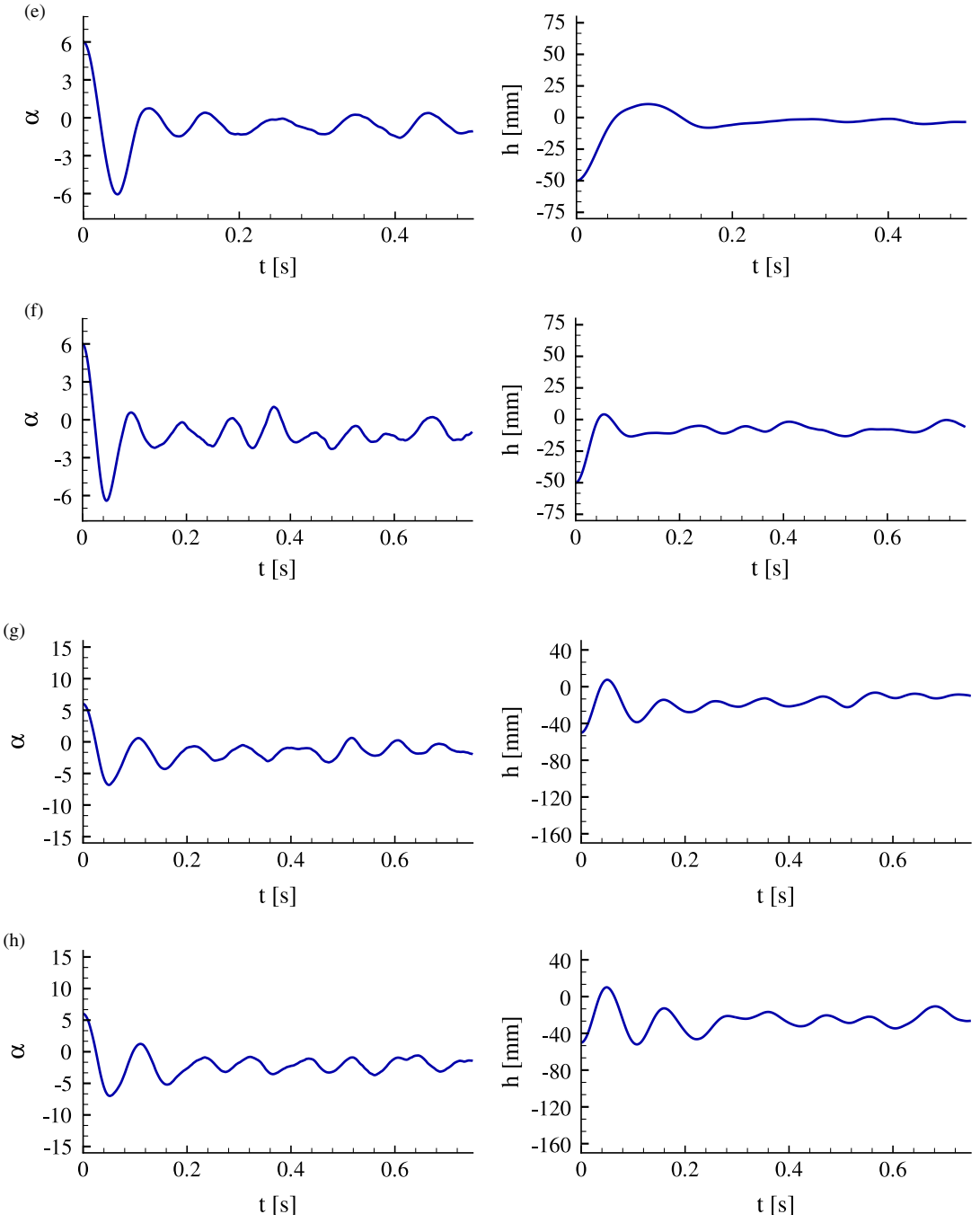

Fig. 10. (*Continued*)

static displacement in Figs. 10(a)–(k) are in agreement with the divergence instability predicted by NASTRAN calculations.

The fluid flow patterns of the velocity and pressure near the vibrating airfoil computed for time instants $t = 0.14$, 0.21, 0.40, 0.47, 0.53, 0.6, 0.65, 0.72, 0.78, 0.84, 0.89, 0.96, 1.02, and 1.08 s are shown in Figs. 11 and 12. These results were obtained in the case of the far field velocity $U_\infty = 40\,\mathrm{m/s}$ and the initial angle of attack $\alpha_0 = 3^\circ$. It is possible to see the development of vortices leaving the airfoil. The angles α of rotation, corresponding to all chosen time instants, are marked in Fig. 13.

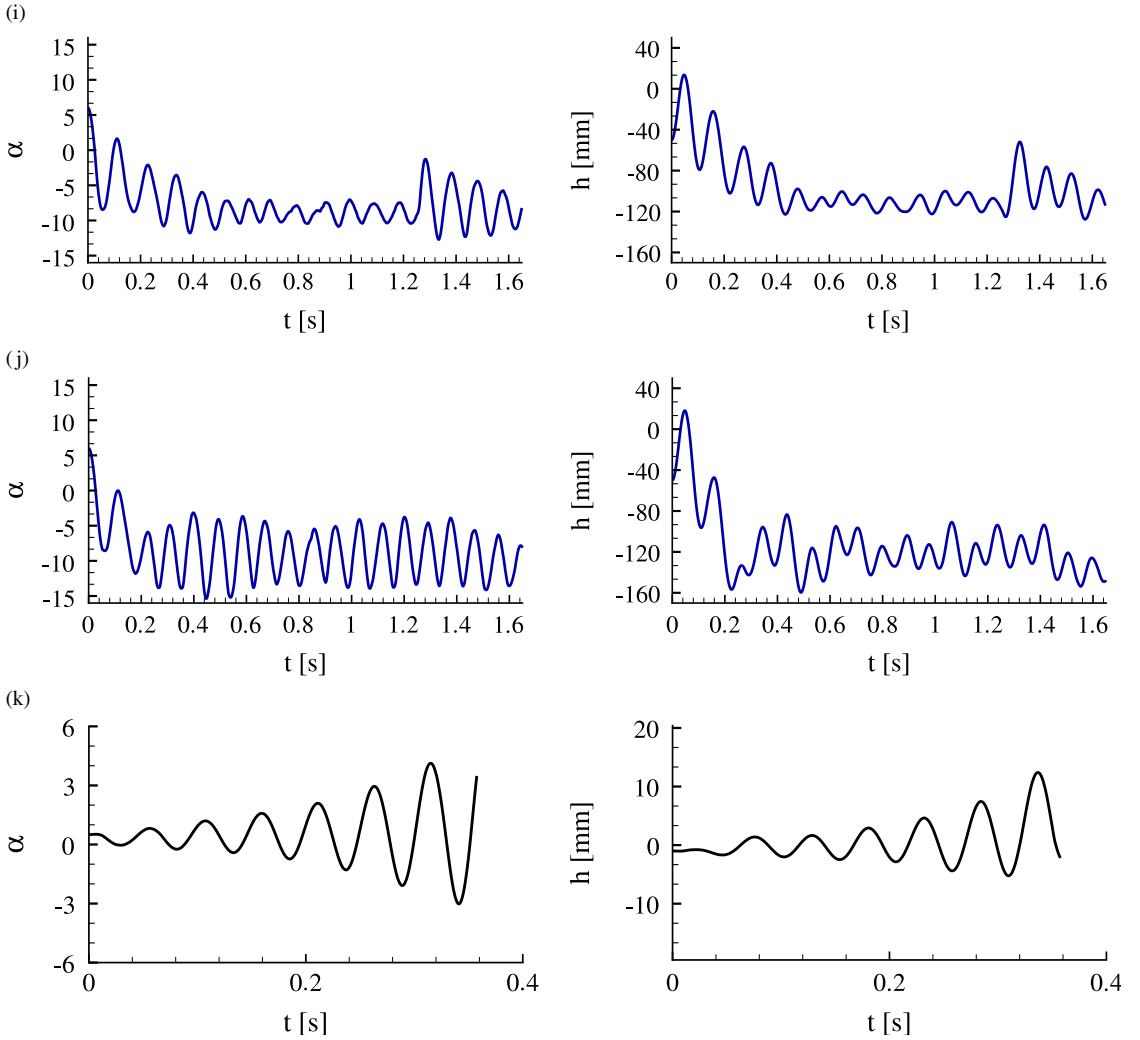

Fig. 10. (*Continued*)

Table 1
The results obtained by NASTRAN code [see Čečrdle and Maleček (2002)]

Predominant	Eigenfrequency for	Critical flow	Instability type	Flutter
Translation	$f_1 = 5.537$	$U_\infty = 37.7$	Divergence	0
Rotation	$f_2 = 13.98$	$U_\infty = 42.4$	Flutter	8.93

The computations were performed on the computer Intel Pentium 1.6–2.4 GHz with RAM 1 GB. The physical time step was chosen in the form $\Delta t = c/(100U_\infty)$. The CPU time increases with increasing U_∞. For example, the CPU time for the computation of a sequence of the length 0.5 s was approximately 24 h in the case of the far field velocity $U_\infty = 30$ m/s. This indicates that for obtaining long time sequences it will be necessary to develop a fast computational code, based on parallelization of the worked out technique, using, e.g., the domain decomposition method and combined with a fast solver for large linear systems.

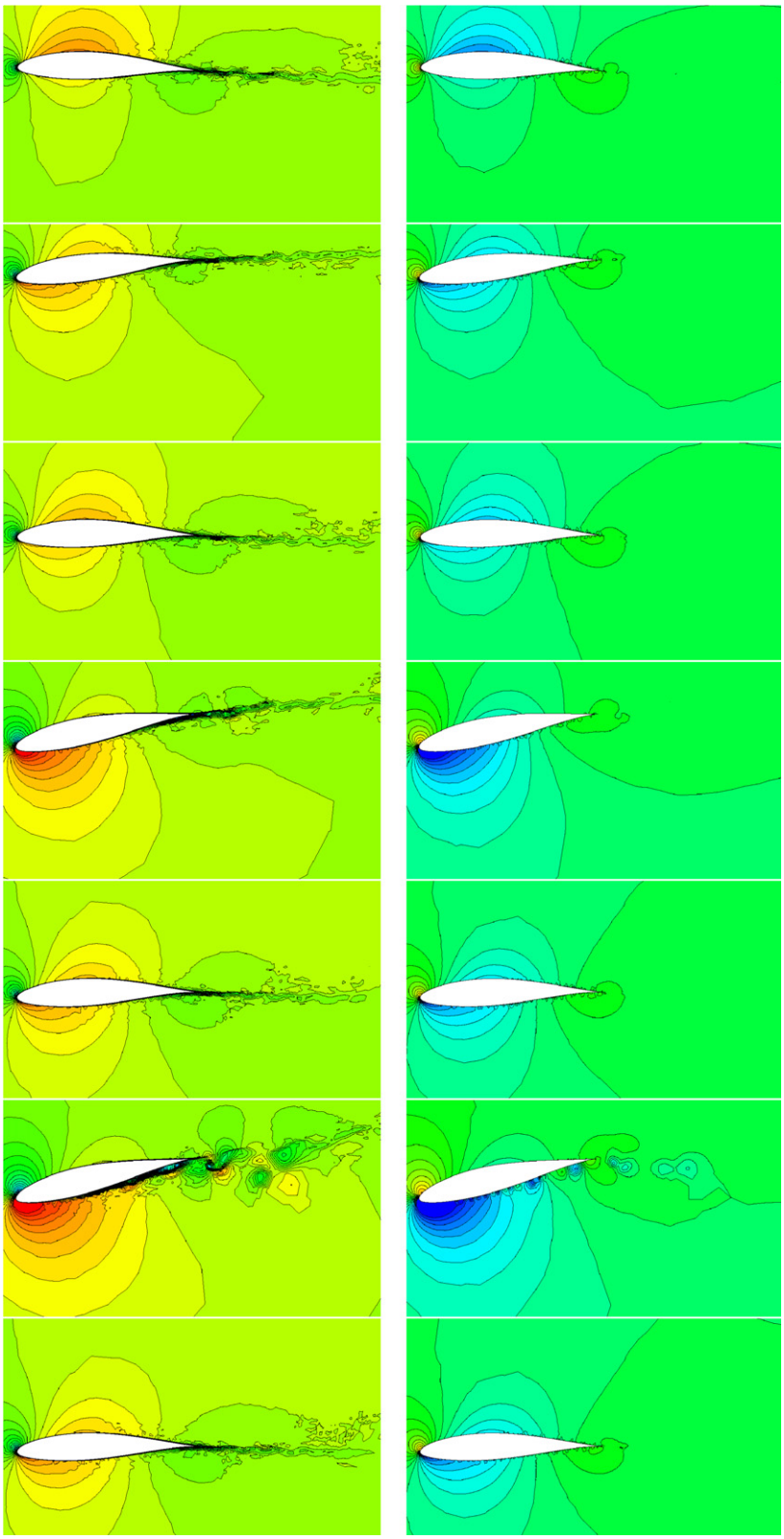

Fig. 11. The distribution of the velocity (left) and the pressure (right) at time instants $t = 0.14$, 0.21, 0.40, 0.47, 0.53, 0.6, and 0.65 s for $U_\infty = 40\,\mathrm{m/s}$ and $\alpha_0 = 3^\circ$.

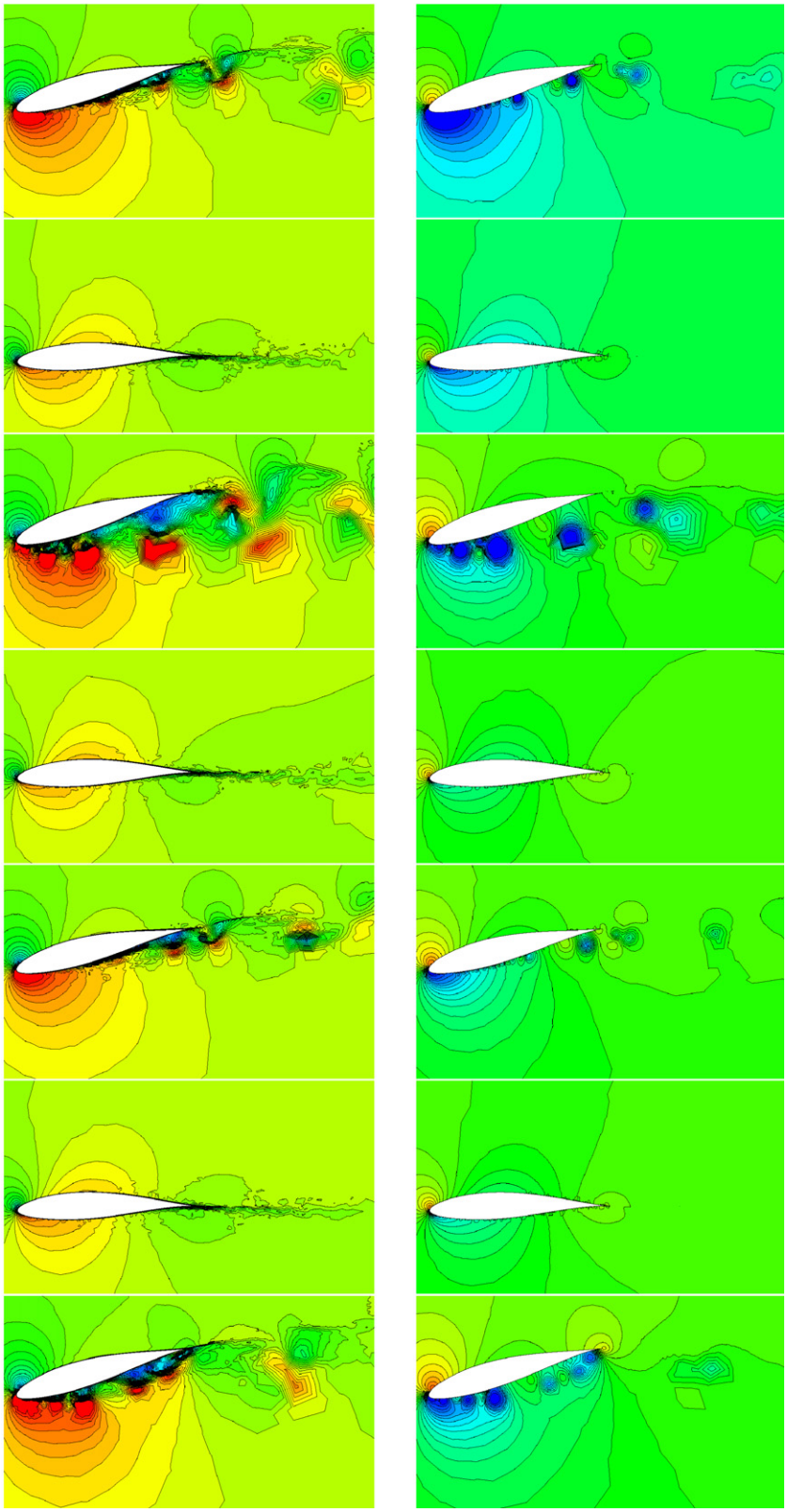

Fig. 12. The distribution of the velocity (left) and the pressure (right) at time instants $t = 0.72, 0.78, 0.84, 0.89, 0.96, 1.02$, and 1.08 s for $U_\infty = 40$ m/s and $\alpha_0 = 3^\circ$.

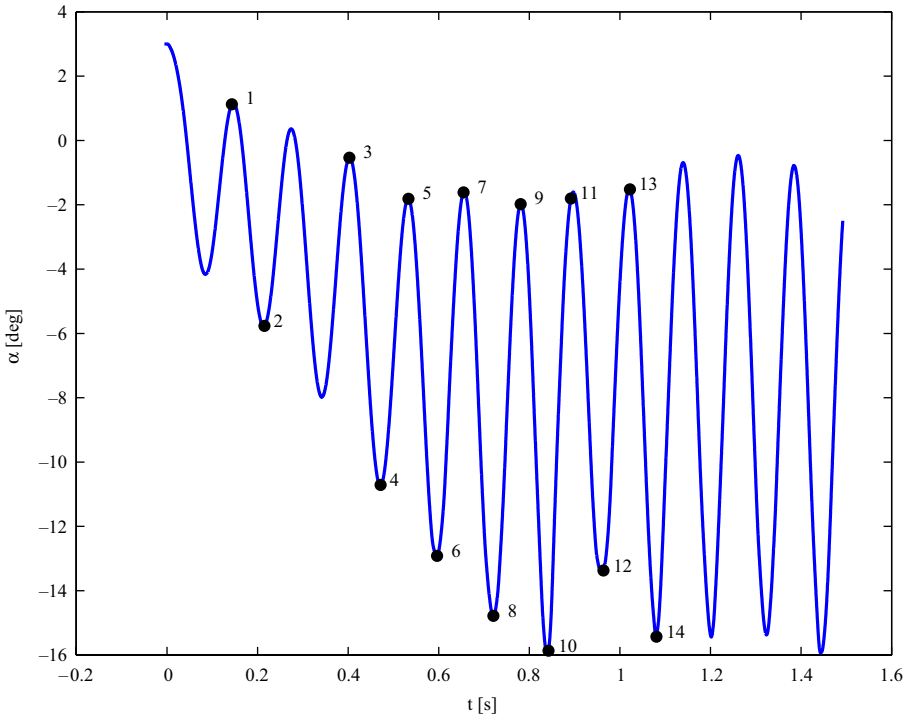

Fig. 13. The rotation angles α in dependence on time for $U_\infty = 40\,\mathrm{m/s}$ and $\alpha_0 = 3^\circ$ with marked values corresponding to flow patterns from Figs. 11 and 12.

5. Conclusion

The robust finite element method (FEM) for the numerical simulation of interaction of incompressible flow and a vibrating airfoil is presented. It is based on the combination of several techniques: the arbitrary Lagrangian–Eulerian (ALE) formulation of the laminar Navier–Stokes equations, suitable time discretization, the finite element method using velocity/pressure finite element pairs satisfying the Babuška–Brezzi condition, stabilization of the finite element scheme, linearization of the discrete nonlinear problem, a fast linear solver, the numerical scheme for the solution of ordinary differential equations describing the vibrations of the airfoil and sufficiently accurate method for the evaluation of fluid dynamical forces acting on the airfoil. The method presented in this paper uses the laminar model and the turbulence modelling is not applied here.

The obtained numerical results are comparable with experimental data as well as with the NASTRAN computations. They indicate that the FEM for the ALE formulation of the Navier–Stokes equations in time dependent domains, coupled with a structural system, is applicable for flows with high Reynolds numbers, provided a proper stabilization of the finite element method, well designed mesh and an efficient linear solver are used.

Acknowledgements

The authors acknowledge the financial support of the Granting Agency of the Academy of Sciences of the Czech Republic by the project No IAA200760613 "Computer Modelling of Aeroelastic Phenomena for Real Fluid Flowing past Vibrating Airfoils Particularly after the Loss of System Stability". This research was also partly supported under the Research Plans MSM 6840770003 (P. Sváček) and MSM 0021620839 (M. Feistauer) of the Ministry of Education of the Czech Republic.

Appendix A

A.1. Nonlinear equations of airfoil motion for large vibration amplitudes

A solid flexibly supported airfoil is shown in Figs. A1, A2 and A3. In Fig. A1 the position of the elastic axis (*EO*), the centre of gravity (*T*) and the airfoil chord (*c*) are sketched. The airfoil can be vertically displaced and rotated. Fig. A2 shows the elastic support of the airfoil on translational and rotational springs.

The pressure and viscous forces acting on the vibrating airfoil are determined by the components of the stress tensor (9) and result in the lift force $L(t)$ and the torsional moment $M(t)$ given by (8). The airfoil in neutral and deformed positions is shown in Fig. A3, from where it follows that the horizontal and vertical displacements of any point on the airfoil chord can be expressed as

$$u = x(1-\cos\alpha), \quad w = h + x\sin\alpha, \tag{A.1}$$

respectively. Here x denotes the local coordinate measured along the airfoil chord c from the elastic axis. The kinetic energy E_K of the airfoil has the form

$$E_K = \int_c \frac{1}{2}\left[\left(\frac{\partial w}{\partial t}\right)^2 + \left(\frac{\partial u}{\partial t}\right)^2\right]\rho_S(x)\,\mathrm{d}x = \frac{1}{2}\left[\int_c (\dot h + x\dot\alpha\cos\alpha)^2 + (x\dot\alpha\sin\alpha)^2\right]\rho_S(x)\,\mathrm{d}x, \tag{A.2}$$

where ρ_S denotes the density of the airfoil per unit length. With further rearrangement of Eq. (A.2) we obtain

$$\begin{aligned} E_K &= \frac{1}{2}\dot h^2\int_c \rho_S(x)\,\mathrm{d}x + \dot h\dot\alpha\cos\alpha\int_c x\rho_S(x)\,\mathrm{d}x + \frac{1}{2}\dot\alpha^2\cos^2\alpha\int_c x^2\rho_S(x)\,\mathrm{d}x + \frac{1}{2}\dot\alpha^2\sin^2\alpha\int_c x^2\rho_S(x)\,\mathrm{d}x \\ &= \frac{1}{2}\dot h^2 m + \dot h\dot\alpha\cos\alpha S_\alpha + \frac{1}{2}\dot\alpha^2 I_\alpha, \end{aligned} \tag{A.3}$$

where

$m = \int_c \rho_S(x)\,\mathrm{d}x$ is the mass of the airfoil,

$S_\alpha = \int_c x\rho_S(x)\,\mathrm{d}x$ is the static moment around the elastic axis *EO*,

$I_\alpha = \int_c x^2\rho_S(x)\,\mathrm{d}x$ is the inertia moment around the elastic axis *EO*.

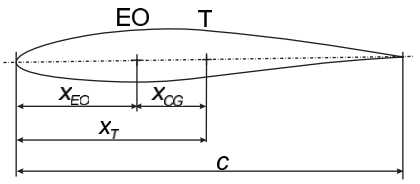

Fig. A1. The position of the elastic axis (*EO*), the centre of gravity (*T*) and the airfoil chord (*c*).

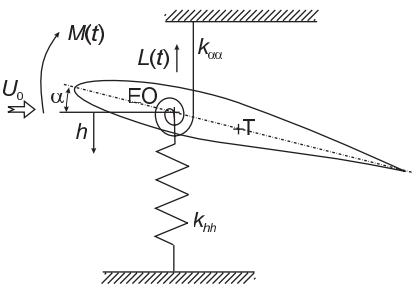

Fig. A2. The elastic support of the airfoil on translational and rotational springs.

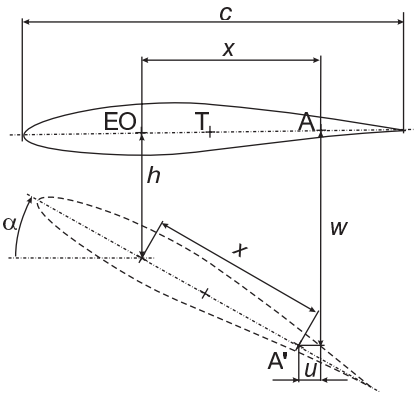

Fig. A3. The airfoil in neutral and deformed position.

The potential energy V of the airfoil is

$$V = \frac{1}{2}k_{hh}h^2 + \frac{1}{2}k_{\alpha\alpha}\alpha^2, \tag{A.4}$$

where k_{hh} and $k_{\alpha\alpha}$ are the bending stiffness and torsional stiffness, respectively.

Kinetic and potential energy have to satisfy the Lagrange equations

$$\frac{\mathrm{d}}{\mathrm{d}t}\frac{\partial E_K}{\partial \dot{q}_j} - \frac{\partial E_K}{\partial q_j} + \frac{\partial V}{\partial q_j} = Q_j, \tag{A.5}$$

where q_j $(j = 1, 2)$ are generalized coordinates, i.e. h and α in our case, and Q_j are generalized forces, i.e. the aerodynamic force $L(t)$ and the moment $M(t)$. Thus, for $j = 1, 2$ we have

$$\frac{\mathrm{d}}{\mathrm{d}t}[\dot{h}m + \dot{\alpha}\cos\alpha S_\alpha] + k_{hh}h = -L(t), \quad \frac{\mathrm{d}}{\mathrm{d}t}[\dot{h}\cos\alpha S_\alpha + \dot{\alpha}I_\alpha] + \dot{h}\dot{\alpha}\sin\alpha S_\alpha + k_{\alpha\alpha}\alpha = M(t). \tag{A.6}$$

Differentiation with respect to time in Eq. (A.6) yields the nonlinear equations of motion of the airfoil

$$m\ddot{h} + S_\alpha\ddot{\alpha}\cos\alpha - S_\alpha\dot{\alpha}^2\sin\alpha + k_{hh}h = -L(t), \quad S_\alpha\ddot{h}\cos\alpha + I_\alpha\ddot{\alpha} + k_{\alpha\alpha}\alpha = M(t). \tag{A.7}$$

For small values of the angle α and of its derivative $\dot{\alpha}$ (i.e., $\sin\alpha \approx \alpha$, $\cos\alpha \approx 1$, $\dot{\alpha}\alpha \approx 0$), Eqs. (A.7) yield the well known linearized system [see, e.g., Dowell (1995)]

$$m\ddot{h} + S_\alpha\ddot{\alpha} + k_{hh}h = -L(t), \quad S_\alpha\ddot{h} + I_\alpha\ddot{\alpha} + k_{\alpha\alpha}\alpha = M(t). \tag{A.8}$$

Including viscous damping terms leads to the governing equations in the form (7) and (6).

References

Akbari, M.H., Price, S.J., 2000. Simulation of the flow over elliptic airfoils oscillating at large angles of attack. Journal of Fluids and Structures 14, 757–777.

Akbari, M.H., Price, S.J., 2003. Simulation of dynamic stall for a NACA 0012 airfoil using a vortex method. Journal of Fluids and Structures 17, 855–874.

Benetka, J., Kladrubský, J., Valenta, R., 1998. Measurement of NACA 0012 profile in a slotted measurement section. Technical Report R-2909/98, Aeronautical Research and Test Institute, Prague, Letňany (in Czech).

Čečrdle, J., Maleček, J., 2002. Verification FEM model of an aircraft construction with two and three degrees of freedom. Technical Report R-3418/02, Aeronautical Research and Test Institute, Prague, Letňany (in Czech).

Davis, T.A., Duff, I.S., 1999. A combined unifrontal/multifrontal method for unsymmetric sparse matrices. ACM Transactions on Mathematical Software 25, 1–19.

Dolejší, V., 2001. Anisotropic mesh adaptation technique for viscous flow simulation. East–West Journal of Numerical Mathematics 9, 1–24.

Dowell, E.H., 1995. A Modern Course in Aeroelasticity. Kluwer Academic Publishers, Dodrecht.

Farhat, C., Lesoinne, M., Maman, N., 1995. Mixed explicit/implicit time integration of coupled aeroelastic problems: three field formulation, geometric conservation and distributed solution. International Journal for Numerical Methods in Fluids 21, 807–835.

Feistauer, M., Felcman, J., Straškraba, J., 2003. Mathematical and Computational Methods for Compressible Flow. Clarendon Press, Oxford.

Fořt, J., Fürst, J., Jirásek, A., Kladrubský, M., Kozel, K., 2002. Numerical solution of 2D and 3D transonic flows over an airfoil and wing. In: Sobieczky, H. (Ed.), Proceedings of Symposium Transonicum IV. DLR, Kluwer Academic Publishers, Göttingen, pp. 211–216.

Fürst, J., Janda, M., Kozel, K., 2001. Finite volume solution of 2D and 3D Euler and Navier–Stokes equations. In: Neustupa, J., Penel, P. (Eds.), Mathematical Fluid Mechanics. Birkhäuser Basel, pp. 173–193

Gelhard, T., Lube, G., Olshanskii, M.A., Starcke, J.-H., 2005. Stabilized finite element schemes with LBB-stable elements for incompressible flows. Journal of Computational and Applied Mathematics 177, 243–267.

Gilliatt, H.C., Strganac, T.W., Kurdila, A.J., 2003. An investigation of internal resonance in aeroelastic systems. Nonlinear Dynamics 31, 1–22.

Girault, V., Raviart, P.-A., 1986. Finite Element Methods for Navier–Stokes Equations. Springer, Berlin.

Gresho, P.M., Sani, R.L., 2000. Incompressible Flow and the Finite Element Method. Wiley, Chichester.

Heo, H., Cho, Y.H., Kim, D.J., 2003. Stochastic control of flexible beam in random flutter. Journal of Sound and Vibration 267, 335–354.

Holmes, P., Marsden, J.E., 1977. Bifurcation to divergence and flutter in flow-induced oscillations: an infinite dimensional analysis. In: Control of Distributed Parameter Systems, Proceedings of Second IFAC Symposium. Coventry, Great Britain, pp. 133–145.

Honzátko, R., Kozel, K., Horáček, J., 2004. Numerical solution of flow through a cascade and over a profile with dynamical and aeroelastic effects. In: de Langre, E., Axisa, F. (Eds.), Flow Induced Vibration, vol. 2. Ecole Polytechnique, France, pp. 377–382.

Horáček, J., 2003. Nonlinear formulation of oscillations of a profile for aero-hydroelastic computations. In: Dobiáš, I. (Ed.), Dynamics of Machines. Prague, Institute of Thermomechanics, AS CR, pp. 51–56.

Le Tallec, P., Mouro, J., 2001. Fluid structure interaction with large displacements. Computer Methods in Applied Mechanics and Engineering 190, 3039–3067.

Lube, G., 1994. Stabilized Galerkin finite element methods for convection dominated and incompressible flow problems. Numerical Analysis and Mathematical Modelling 29, 85–104.

NACA, 1945. Summary of airfoil data. Technical Report 824, NACA, Washington.

Naudasher, E., Rockwell, D., 1994. Flow-Induced Vibrations. A.A. Balkema, Rotterdam.

Nomura, T., Hughes, T.J.R., 1992. An arbitrary Lagrangian–Eulerian finite element method for interaction of fluid and a rigid body. Computer Methods in Applied Mechanics and Engineering 95, 115–138.

Otto, F.C., Lube, G., 1998. Non-overlapping domain decomposition applied to incompressible flow problems. Contemporary Mathematics 218, 507–514.

Půlpitel, L., 1984. Experimental investigation of conditions for the origin of torsional self-oscillations of a blade on a model facility with a big blade. Technical Report No. 4 OTE 9961-800, ČKD Blansko, 44 (in Czech).

Quarteroni, A., Valli, A., 1999. Domain Decomposition Methods for Partial Differential Equations. Oxford University Press, Oxford.

Singh, S., Brenner, M., 2003. Limit cycle oscillation and orbital stability in aeroelastic systems with torsional nonlinearity. Nonlinear Dynamics 31, 435–450.

Sváček, P., Feistauer, M., 2004. Application of a stablized FEM to problems of aeroelasticity. In: Feistauer, M., Dolejší, V., Knobloch, P., Najzar, K. (Eds.), Numerical Mathematics and Advanced Applications, ENUMATH2003. Springer, Heidelberg, pp. 796–805.

Triebstein, H., 1986. Steady and unsteady transonic pressure distributions on NACA 0012. Journal of Aircraft 23, 213–219.

Tuncer, I., Wu, J., Wang, C., 1990. Theoretical and numerical studies of oscillating airfoils. AIAA Journal 28 (9), 1615–1624.

Turek, S., 1999. Efficient Solvers for Incompressible Flow Problems: An Algorithmic and Computational Approach. Springer, Berlin.

Verfürth, R., 1984. Error estimates for mixed finite element approximation of the Stokes equations. RAIRO Analyse Numérique/Numerical Analysis 18, 175–182.